



January 2017

Synthesis And Characterization Of Max Ceramics (MAXCERs)

Johnny Carl Nelson

Follow this and additional works at: <https://commons.und.edu/theses>

Recommended Citation

Nelson, Johnny Carl, "Synthesis And Characterization Of Max Ceramics (MAXCERs)" (2017). *Theses and Dissertations*. 2298.
<https://commons.und.edu/theses/2298>

This Thesis is brought to you for free and open access by the Theses, Dissertations, and Senior Projects at UND Scholarly Commons. It has been accepted for inclusion in Theses and Dissertations by an authorized administrator of UND Scholarly Commons. For more information, please contact zeinebyousif@library.und.edu.

Synthesis and Characterization of MAX Ceramics (MAXCERs)

by

Johnny Carl Nelson

Bachelor of Science, University of North Dakota

A Thesis

Submitted to the Graduate Faculty

of the

University of North Dakota

in partial fulfillment of the requirements

for the degree of

Master of Science


Grand Forks, North Dakota

July

2017

Copyright © 2017 Johnny Nelson


This thesis, submitted by Johnny C Nelson in partial fulfillment of the requirements for the Degree of Master of Science from the University of North Dakota, has been read by the Faculty Advisory Committee under whom the work has been done and is hereby approved.



Dr. Surojit Gupta, PhD



Dr. Matthew Cavalli, PhD, PE

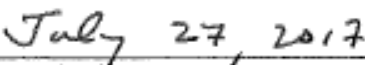


Dr. Clement Tang, PhD

This thesis meets the standards for appearance, conforms to the style and format requirements of the School of Graduate Studies of North Dakota, and is hereby approved.



Grant McGimpsey
Dean of the Graduate School



Date 7/27/2017

PERMISSION

Title Synthesis and Characterization of MAX Reinforced Ceramics (MAXCERs)

Department Mechanical Engineering

Degree Master of Science

In presenting this thesis in fulfillment of the requirements for a graduate degree from the University of North Dakota, I agree that the library of this University shall make it freely available for inspection. I further agree that permission for extensive copying for scholarly purposes may be granted by the professor who supervised my thesis work or, in his absence, by the chairperson of the department or the dean of the Graduate School. It is understood that any copying or publication or other use of this thesis or part thereof for financial gain shall not be allowed without my written permission. It is also understood that due recognition shall be given to me and to the University of North Dakota in any scholarly use which may be made of any material in my thesis.

Signature Johnny C Nelson

Date 07/27/2017

TABLE OF CONTENTS

TITLE	PAGE
LIST OF FIGURES.....	viii
ACKNOWLEDGEMENTS.....	xi
ABSTRACT.....	xii
CHAPTER	
I. INTRODUCTION.....	1
1.1 MAX Phase.....	1
1.2 Ceramics.....	4
1.3 MAX-Ceramics (MAXCERs).....	5
II. SYNTHESIS AND CHARACTERIZATION OF Ti_3SiC_2 - Al_2O_3 , BN, and B_4C MAXCER COMPOSITES.....	7
2.1 Experimental Details.....	7
2.2 Results and Discussion.....	9
2.3 Conclusions.....	16
III. TiB_2 - Ti_3SiC_2 MAXCER COMPOSITES	
3.1 Introduction.....	17
3.2 Experimental Methods.....	18
3.3 Results and Discussion.....	20
3.4 Scope for Future Studies.....	28
APPENDIX.....	29

REFERENCES.....29

LIST OF FIGURES

FIGURE	PAGE
1.1. MAX phase elemental grouping on Periodic Table.....	2
1.2. Dual-type (μ) transitions.....	3
1.3. Dual stage tribological response graphs for fine grained Ti_3SiC_2	4
2.1. FESEM SE micrographs of, (a) sintered Ti_3SiC_2 , (b) BSE image of the same region, (c) $312Si-1\%Al_2O_3$, (d) BSE image of the same region, (e) $312Si-6\%Al_2O_3$, and (f) BSE image of the same region.....	9
2.2. FESEM SE micrographs of, (a) $312Si-1\%B_4C$, (d) BSE image of the same region, (e) $312Si-5\%B_4C$, and (f) BSE image of the same region.....	10
2.3. FESEM SE micrographs of, (a) $312Si-1\%BN$, (d) BSE image of the same region, (e) $5\%BN$, and (f) BSE image of the same region.....	10
2.4. XRD patterns of, (a) $Ti_3SiC_2-Al_2O_3$ composites, (b) $Ti_3SiC_2- B_4C$ composites, and (c) Ti_3SiC_2-BN composites.....	12
2.5. Plot of, (a) relative density, and (b) hardness versus the vol(%) additions of ceramic particulates.....	13
2.6. Plot of friction coefficient versus distance of, (a) $Ti_3SiC_2-1wt\%Ni$, (b) $312Si-1\%Al_2O_3$, (c) $312Si-1\%B_4C$ and (d) $312Si-1\%BN$	14
2.7. Plot of friction coefficient (μ) versus distance of, (a) $312Si-6\%Al_2O_3$, (b) $312Si-5\%B_4C$, (c) $312Si-5\%BN$, and (d) Transition Distance (TD) versus additives (vol%).....	15
2.8. BSE SEM micrographs of, (a) stainless steel, and (b) $312Si-5\%BN$ surface after tribological testing.....	16
3.1. SE SEM images of (a) TiB_2 , (b) BSE of the same image (dark phase is the porosity in which diamond polish has entered the pores), (c) $TiB_2-10\%Ti_3SiC_2$, (d) BSE of the same image,	

(e) TiB ₂ -30%Ti ₃ SiC ₂ , (f) BSE of the same image, (g) TiB ₂ -50% Ti ₃ SiC ₂ , and (h) BSE of the same image.....	22
3.2. XRD analysis of (a) TiB ₂ , (b) TiB ₂ -10%Ti ₃ SiC ₂ , (c) TiB ₂ -30%Ti ₃ SiC ₂ , and (d) TiB ₂ -50%Ti ₃ SiC ₂	23
3.3. Relative Density and Hardness versus MAX Content (vol%).....	24
3.4. Friction coefficient versus Ti ₃ SiC ₂ vol%.....	25
3.5. Friction coefficient versus sliding distance.....	25
3.6. Wear rate versus Ti ₃ SiC ₂ content (vol%).....	26
3.7. SEM micrograph of tribofilm formed on TiB ₂ -10%Ti ₃ SiC ₂ surface.....	27
3.8. Experimental runs of friction versus sliding distance (1000m) of TiB ₂ -50%Ti ₃ SiC ₂	27

ACKNOWLEDGEMENTS

I am indebted to the Department of Mechanical Engineering of UND for allowing me this opportunity to pursue research in the field of Material Science. I would like to express my respect and admiration for Dr. Surojit Gupta as he patiently guided my research during my schedule of working full time and being off-campus. Furthermore I have much gratitude for the tremendous knowledge that he is willing to share with all of his students. I am grateful for my fellow graduate students, without which I would not have succeeded. Specifically I would like to mention the support of Matt Fuka, Madison Olson, Dan Berg, Sujan Goush and Faisal Al Anazi. I would like to mention the support of Dr. Matthew Cavalli for sitting on my committee and helping me to develop an appreciation for material science. Finally, I would also like to thank Dr. Clement Tang for his review of this thesis report.

ABSTRACT

This research has focused on the design and development of novel multifunctional MAX reinforced ceramics (MAXCERs). These MAXCERs were manufactured with 1-50 vol% ratios of ceramics to MAX phases. Chapter II reports on the synthesis and tribological behavior of Ti_3SiC_2 matrix composites by incorporating (1 and 6 vol%) Al_2O_3 , (1 and 5 vol%) BN, and (1 and 5 vol%) B_4C ceramic particulate additives in the matrix. All the composites were fabricated by pressureless sintering by using ~1 wt% Ni as a sintering agent at 1550 °C for 2 hours. SEM and XRD studies showed that Al_2O_3 is relatively inert in the Ti_3SiC_2 matrix whereas BN and B_4C reacted significantly with the Ti_3SiC_2 matrix to form TiB_2 . Detailed tribological studies showed that Ti_3SiC_2 -1wt%Ni (baseline) samples showed dual type tribological behavior where the friction coefficient (μ) was low (~0.2) during stage 1, thereafter μ increased sharply and transitioned into stage 2 (~0.8). The addition of Al_2O_3 as an additive had little effect on the tribological behavior, but the addition of B_4C and BN was able to enhance the tribological behavior by increasing the transition distance (TD). Chapter III reports on the synthesis and tribological behavior of TiB_2 matrix composites by incorporating (10, 30, and 50 vol%) Ti_3SiC_2 ceramic particulate additives in the matrix. The fabrication parameters were similar to the Ti_3SiC_2 samples from Chapter II. There was minimal reaction between the TiB_2 and the Ti_3SiC_2 . Detailed tribological studies showed that TiB_2 (baseline) and TiB_2 -10% Ti_3SiC_2 samples showed an average μ of ~0.29 and ~0.28, respectively. TiB_2 -30% Ti_3SiC_2 and TiB_2 -50% Ti_3SiC_2 showed dual-type tribological behavior where μ was low (~0.25) during stage 1, thereafter μ increased gradually and transitioned into stage 2 (~0.6). Low wear rates were seen for all samples.

CHAPTER I

INTRODUCTION

1.1 - MAX Phase

MAX phases exhibit a variety of unique properties, often combining good attributes of both metallic and ceramic elements [1]. Metallic elements exhibit excellent room temperature strength, but oxidize and soften easily at higher temperatures [1]. Ceramics, as a material group, exhibit excellent high-temperature properties, good chemical stability, and oxidation resistance [2,3]. Unfortunately, ceramics have low toughness, brittleness, and are prone to thermal shock. Thus the benefits of combining both metallic and ceramic properties are evident. There is a great need in modern industry for tribological systems that are able to reliably function in harsh conditions. MAX-phase materials are seen as an attractive choice of material in these types of engineering applications, where severe thermal and mechanical conditions are present in an oxidative environment.

The $M_{n+1}AX_n$ (MAX) phases (over 70+ phases) are thermodynamically stable layered hexagonal (space group D_{6h}^4 -P6₃/mmc) with two formula units per cell [3-5]. These phases possess a $M_{n+1}AX_n$ chemistry, where n is 1, 2, or 3, M is an early transition metal element, A is an A-group element and X is C or N. Figure 1 shows the general grouping of these phases. Some early research has suggested that Ti_3SiC_2 , due to its layered structure, may have good solid-lubricant qualities [3]. Later, Myhra et al. [6] also showed that by using a lateral force

microscope with a Si₃N₄ tip, the friction coefficients, μ , of the basal planes were ultra-low ($2-5 \times 10^{-3}$), but the μ 's of non-basal planes were much higher. Interestingly, the tribological behavior

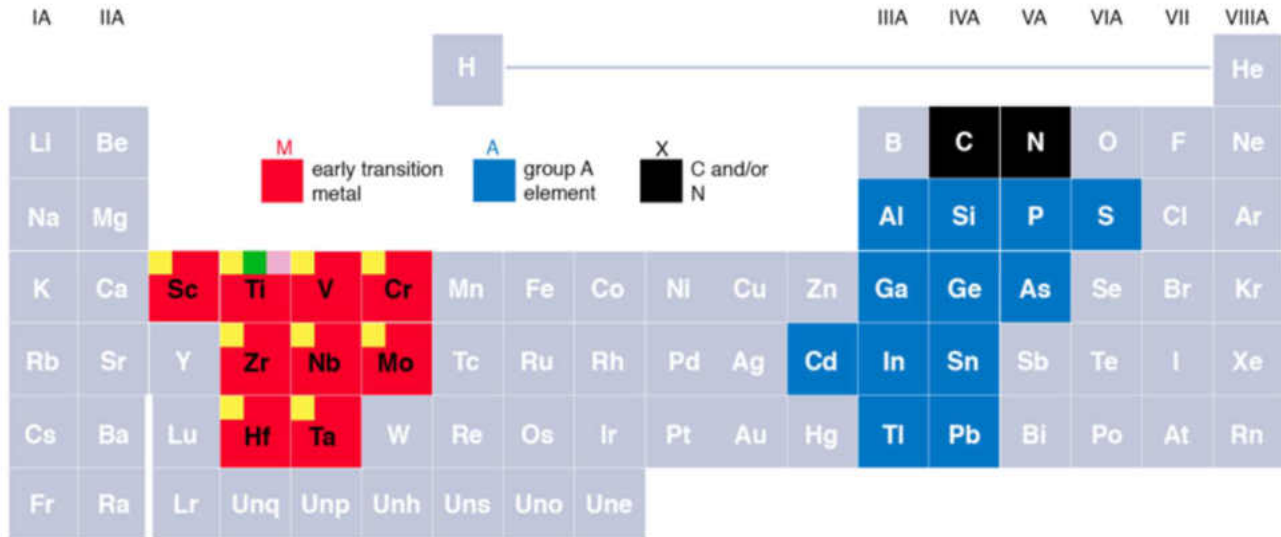


Figure 1.1: MAX phase elemental grouping on Periodic Table [3]

of polycrystalline samples showed different results. For example, El-Raghy et al. [7] showed that both coarse-grained, CG ($\sim 25-50 \mu\text{m}$) and fine-grained, FG ($\sim 4 \mu\text{m}$) polycrystalline Ti₃SiC₂ samples during testing by using a pin-on-disc method against a 9.5 mm diameter 440C steel ball, a load of 5 N, with a sliding speed of 0.1 m/s showed low μ , initially, which increased linearly from 0.15 to 0.4 and then attained a steady state value of 0.8. Due to third body abrasion, the average sliding wear rates were high, $1.34 \times 10^{-3} \text{ mm}^3/\text{N m}$ and $4.25 \times 10^{-3} \text{ mm}^3/\text{N m}$, for the FG and CG samples, respectively.

The time dependent friction coefficients are shown in figure 2(a) and 2(b), which are qualitatively similar. To be noted is the distinct transition stage that can be seen in both graphs [7]. Blau [8] explained this as a friction break-in curve, wherein a tribofilm or coating with lubricating properties wears through to expose a higher friction substrate, as a result of the

transfer of sliding material to the counter-surface, leading to a self-mated, higher friction coefficient condition. However, later research by Souchet et al. [9] studied the dual-type tribology of FG ($\sim 4 \mu\text{m}$) and CG ($\sim 25\text{--}50 \mu\text{m}$) Ti_3SiC_2 samples

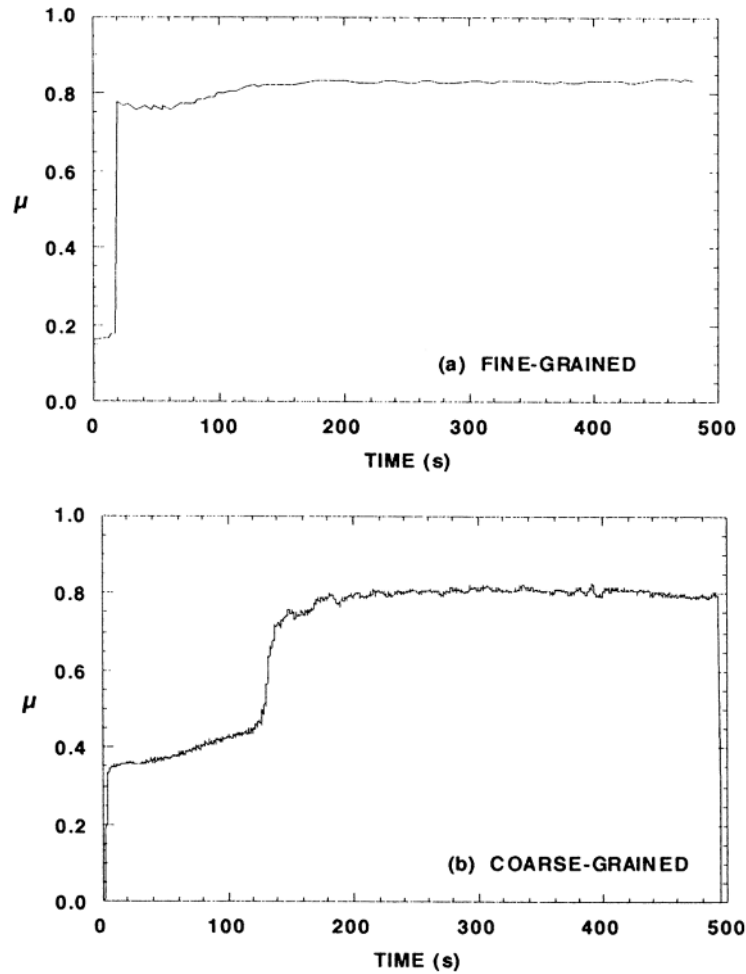


Figure 1.2: Dual-type (μ) transitions [9]

against steel and Si_3N_4 balls by using a reciprocating type tribometer in detail. Souchet et al. [9] concluded that the transition between the two regimes occurred at different times, and depended on various factors such as grain size, type of pin, and normal load applied.

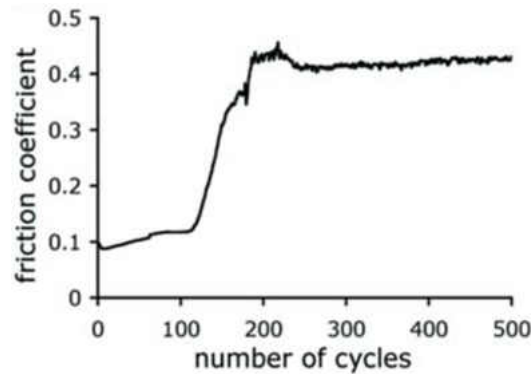


Figure 1.3: Dual stage tribological response graphs for fine grained Ti_3SiC_2 [9].

Several investigators have observed similar dual-type tribological behavior in Ti_3SiC_2 based ceramics [10]. Clearly, due to high wear rate, pristine Ti_3SiC_2 ceramics cannot be used as a coating material for high performance tribological applications.

1.2 - Ceramics

As a class, ceramics are hard, brittle, wear-resistant, prone to thermal shock, refractory, electrically and thermally insulative, chemically stable, oxidation resistant and non-magnetic [11]. Simple ceramics, such as kaolinite, can be formed by heat alone, or by heat and pressure. They are comprised of at least two elements provided at least one of them is a non-metal or a non-metallic elemental solid, and the other element(s) can be a metal(s) or a non-metallic elemental solid(s) [11]. Moving beyond simple ceramics to advanced ceramics, much research has occurred in advanced structural and high strength ceramics starting in the 1970s, propelled in part by rising oil prices [12]. Proposed applications from that period included using ceramics to build Diesel engines and turbines, due to their light weight, high temperature capability, and better environmental resistance. However, as mentioned above, a weakness of ceramics is their

brittle, nonductile behavior, making them prone to catastrophic failure [12]. Since that time there has been continuing research focused on tougher, damage-resistant ceramic materials [12-14].

1.3 - Introduction to MAX-Ceramics (MAXCERs)

The incorporation of a hard phase into a softer matrix to achieve an improved tribological response of lower wear rate and friction coefficient is well known. This concept can be applied across many different kinds of material combinations, such as metal-metal, ceramic-metal, ceramic-ceramic and MAX-ceramic, to name a few. Often these combinations use useful parameters from each composite. An appropriate example would be a metallic element's natural ductility at room temperature, contributing fracture toughness, while also utilizing its ability to form liquid sintering phases at elevated temperatures, assisting with densification [14]. Metal binder such as Al or Co exhibit excellent room temperature strength, but is prone to softening and oxidation [15,16].

Often the matrix is composed of metallic and carbide particles, which stand in relief and provide wear resistance. The ductile softer matrix assists in dispersing the load more uniformly, and provide toughness and fatigue resistance [17]. There is a wide variety of composite percentages among the research. Often when a low percentage is used, it acts as a sintering or binding agent. In general there are two kinds of binders, ceramics (vitrified) and metals [15]. Ceramics binders such as TiC, TiN, and TiB₂ show very good high-temperature properties, and TiC and TiN show excellent oxidation resistance. However, they all have low toughness and are prone to damage at room temperature [15,16]. A review of the literature appears to show little research regarding MAX-ceramic-matrix composites, in contrast to the plentiful research on metal-matrix composites and ceramic-matrix composites. Furthermore, metal-metal and metal-

ceramic-matrix composite research has been occurring for many decades [18-20]. Nonetheless, interesting research on MAX-ceramic composites have occurred.

Li et.al. [15] used high-pressure, high-temperature (HTHP) techniques to combine Ti_3SiC_2 -cBN, using the Ti_3SiC_2 as a binder and reported this material to show great promise as a super hard material. Zheng et.al. [14] reported remarkable improvement in TiB_2 densification by combining 10 wt% Ti_3AlC_2 . Other researchers [21] have suggested that certain borides based on the AlB_2 crystal structure shared similarities with MAX materials. These shared features include a layered structure, showing strongly anisotropic bonding, and having the AlB_2 crystal structure, which belong to space group $P6/mmc$. Similar to nitride and carbide based MAX phases, all of these materials have metallic bonding in the intermetallic layers, but with a much stronger covalent bonding within the boron (or other non-metallic) network.

Overall, this combination of the metallic bonding coupled with the covalent bonding of MAX phase and MAX phase-like materials gives rise to their high melting point, hardness and stiffness [21]. Hence combining these properties with advanced ceramics have the potential for excellent tribological and mechanical properties. The purpose of this research is to study the tribological and mechanical effect on Ti_3SiC_2 with a variety of vol% additions of Al_2O_3 , B_4C , BN , and TiB_2 . These composites will be designated as MAXCERs.

CHAPTER II

SYNTHESIS AND CHARACTERIZATION OF Ti_3SiC_2 - Al_2O_3 , BN, and B_4C MAXCER COMPOSITES

2.1 - Experimental Details

Ti_3SiC_2 powder (-325 mesh, Kanthal, Hallstahammar, Sweden) and calculated concentrations of ceramic powders (Alpha Al_2O_3 powders (nanopowder, Inframat Advanced Materials, Manchester, CT) or BN powders ($\sim 1 \mu\text{m}$, Sigma Aldrich, St. Louis, MO) or B_4C powders ($< 10 \mu\text{m}$, Sigma Aldrich, St. Louis, MO) were dry ball milled (8000 M mixer Mill, SPEX SamplePrep, Metuchen, NJ) for five minutes. All the powders were then poured in a die and were cold-pressed at $\sim 232 \text{ MPa}$ (the cycle was repeated twice) in a $\sim 12.7 \text{ mm}$ die (EQ-Die-12D-B, MTI Corporation, Richmond, CA), and sintered at $1550 \text{ }^\circ\text{C}$ for 120 minutes in a tube furnace with Ar flowing through it (to prevent oxidation). All the MAXCER composites were designed by adding 1 vol% ($312\text{Si}-1\%\text{Al}_2\text{O}_3$ or $312\text{Si}-1\%\text{BN}$ or $312\text{Si}-1\%\text{B}_4\text{C}$), 5 vol% ($312\text{Si}-5\%\text{BN}$ or $312\text{Si}-5\%\text{B}_4\text{C}$), and 6 vol% ($312\text{Si}-6\%\text{Al}_2\text{O}_3$) of ceramic particulates in the Ti_3SiC_2 matrix. In all compositions, $\sim 1 \text{ wt}\%$ Ni of the Ti_3SiC_2 content was added as a sintering aid. In addition, Ti_3SiC_2 with $\sim 1 \text{ wt}\%$ Ni was also fabricated for comparison ($\text{Ti}_3\text{SiC}_2-1\% \text{ Ni}$).

The rule of mixtures was used to calculate the theoretical density of all the composite samples by using the theoretical density of Ti_3SiC_2 and ceramic particulates. The experimental density was also determined from the mass and dimensions of each sample. The relative density was then calculated by normalizing the experimental density with theoretical density. In Ti_3SiC_2 -BN and Ti_3SiC_2 - B_4C composites, it is difficult to calculate the exact theoretical density due to the interfacial reaction and formation of different phases like TiB_2 . For this reason, the density

calculations are based on starting compositions of the precursor powders and should be used for qualitative comparison only. All the composites were polished ($R_a < 1 \mu\text{m}$) and then tested by a Vicker's micro-hardness indenter (Mitutoyo HM-112, Mitutoyo Corporation, Aurora, IL) by loading the samples at $\sim 9.8 \text{ N}$ for 12 seconds, and an average of five readings for each composite system is reported in the text. The phase analysis was performed by XRD (SmartLab, Rigaku, Japan) at a scan rate of $0.05^\circ/\text{min}$ from 20° to 70° . The tribological behavior of the samples were tested by using a block (tab)-on-disc tribometer (CSM Instruments SA, Peseux, Switzerland) at 5 N , $\sim 31 \text{ cm/s}$ linear speed, and $\sim 5 \text{ mm}$ track radius against stainless steel balls. The transition distance (TD) is defined as the distance after which the tribological behavior changed from Type I (low μ) to Type II (high μ). An average of three TDs from different compositions is reported in the text.

The microstructure of the samples was studied by using a JEOL JSM-6490LV Scanning Electron Microscope (SEM JEOL USA, Inc., Peabody, Massachusetts) in Secondary Electron (SE) and Backscattered Electrons (BSE) mode. The chemical information was obtained by X-ray analysis via a Thermo Nanotrace Energy Dispersive X-ray detector with NSS-300e acquisition engine. The accuracy of measuring C is quite low during chemistry analysis by X-ray detector in SEM. All the compositions listed, especially sub-stoichiometric oxides, could very well contain C, which is very difficult to determine experimentally. In this paper, a combination of BSE and X-ray analysis is used to determine the tribochemistry of tribocouples. If a region is determined to be chemically uniform at the micron level then it will be identified with two asterisks as a *microconstituent* to emphasize that these areas are not necessarily single phases. In addition, the presence of C in these tribofilms will be shown by adding $\{C_x\}$ in the composition [4].

2.2 - Results and Discussion

The microstructure of the $\text{Ti}_3\text{SiC}_2\text{-Al}_2\text{O}_3$ composites are shown in Figure 4. The Al_2O_3 particulates are well-dispersed in the Ti_3SiC_2 matrix.

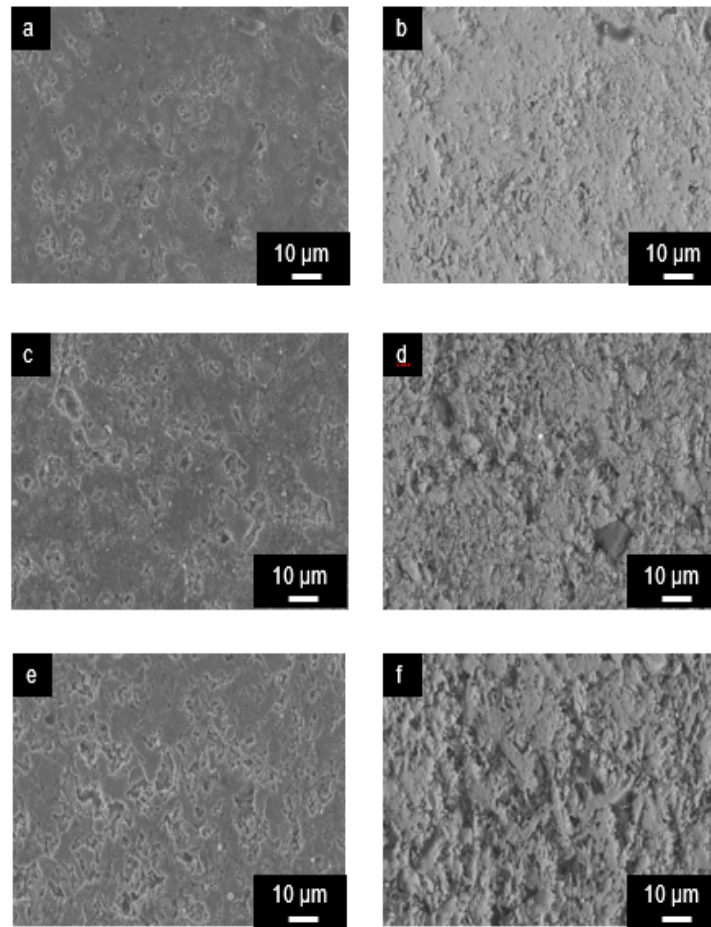


Figure 2.1: FESEM SE micrographs of, (a) sintered Ti_3SiC_2 , (b) BSE image of the same region, (c) $312\text{Si-1}\%\text{Al}_2\text{O}_3$, (d) BSE image of the same region, (e) $312\text{Si-6}\%\text{Al}_2\text{O}_3$, and (f) BSE image of the same region.

Figures 2.2 and 2.3 show the $\text{Ti}_3\text{SiC}_2\text{-B}_4\text{C}$ and $\text{Ti}_3\text{SiC}_2\text{-BN}$ composites, respectively. The microstructures are very heterogeneous and it is difficult to discern individual particles.

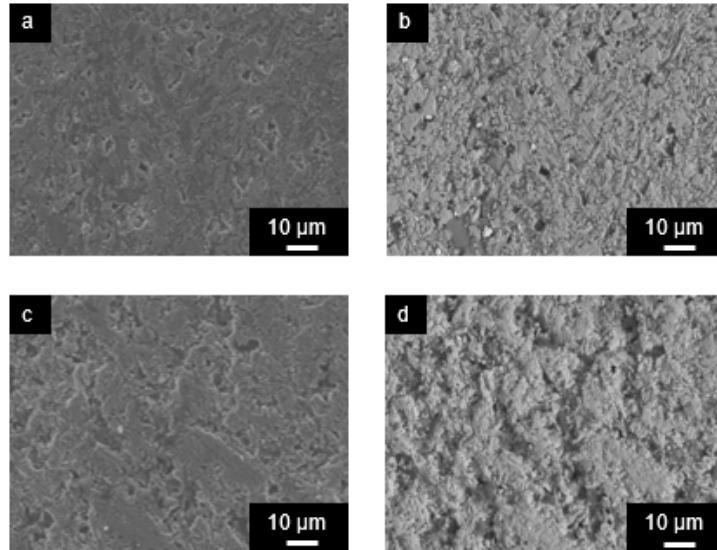


Figure 2.2: FESEM SE micrographs of, (a) $312\text{Si-1\%B}_4\text{C}$, (d) BSE image of the same region, (e) $312\text{Si-5\%B}_4\text{C}$, and (f) BSE image of the same region.

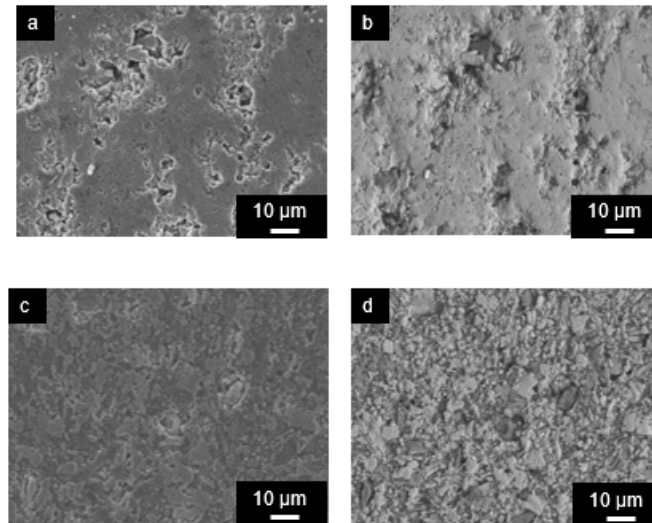


Figure 2.3: FESEM SE micrographs of, (a) 312Si-1\%BN , (d) BSE image of the same region, (e) 312Si-5\%BN , and (f) BSE image of the same region.

Figure 2.4 summarizes the XRD profile of all the compositions. In the $\text{Ti}_3\text{SiC}_2\text{-Al}_2\text{O}_3$ composites (Figure 2.4(a)) – alumina was observed in the XRD peaks which indicate that Al_2O_3 particulates are stable in the Ti_3SiC_2 microstructure. Comparably, Figure 2.4(b) and 2.4(c) show the formation of TiB_2 which indicate that the B_4C and BN are not stable in the Ti_3SiC_2 matrix and result in the formation of TiB_2 .

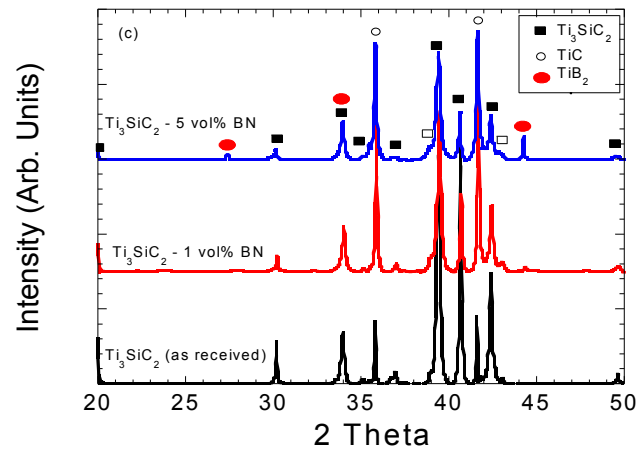
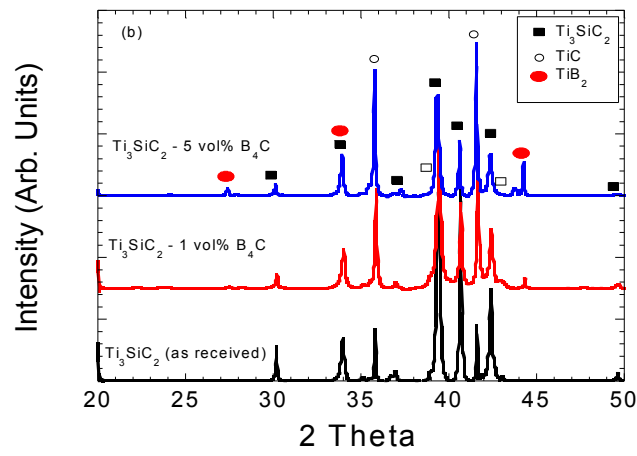
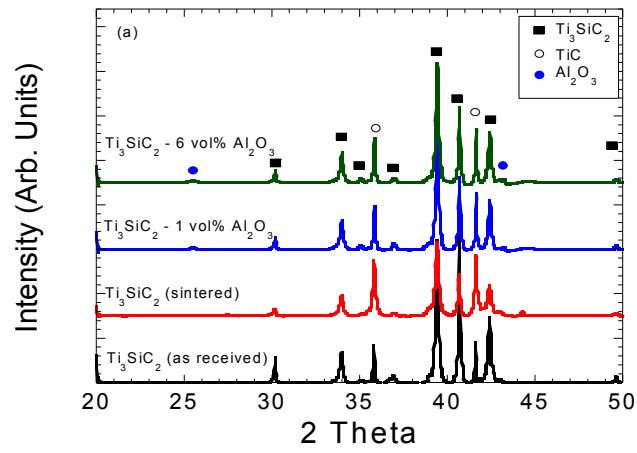


Figure 2.4: XRD patterns of, (a) Ti_3SiC_2 - Al_2O_3 composites, (b) Ti_3SiC_2 - B_4C composites, and (c) Ti_3SiC_2 -BN composites.

Figure 2.5(a) shows the plot of relative density versus the additions of ceramic particulates. It is difficult to calculate the exact theoretical density due to the interfacial reaction and formation of different phases like TiB_2 (Figure 2.4), thus the plot of Figure 2.5(a) is a qualitative comparison. The Ti_3SiC_2 -1wt% Ni samples were predominantly single phase and had a relative density of $\sim 96\%$. The addition of 1 vol% of ceramic particulates had no deleterious effect on the relative density, and the relative density retained similar values. However, the addition of higher vol% (5-6 vol%) of ceramic particulates had a negative effect on the densification, and the resultant samples were porous as compared to Ti_3SiC_2 -1wt% Ni (Figure 2.5(a)). Comparatively, the hardness of Ti_3SiC_2 -1wt% Ni was ~ 3 GPa, it gradually increased to ~ 4 GPa in 312Si-5%BN or 312Si-5%B₄C, and all compositions of the Ti_3SiC_2 -Al₂O₃ composites had a hardness value of ~ 3 GPa (Figure 2.5(b)).

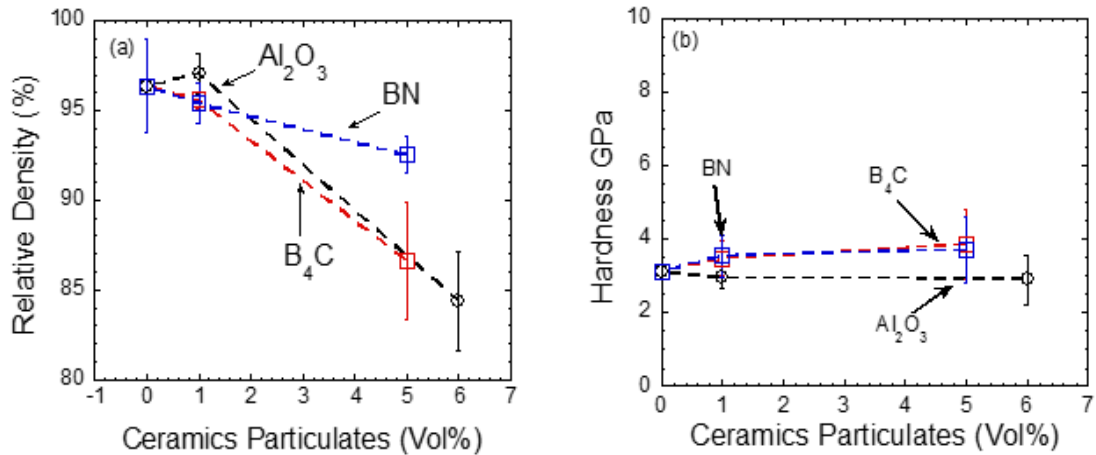


Figure 2.5: Plot of, (a) relative density, and (b) hardness versus the vol(%) additions of ceramic particulates

Figures 2.6-2.7 plot the μ versus sliding distance of different Ti_3SiC_2 based composites. Figure 2.6(a) shows the μ versus sliding distance profile of the Ti_3SiC_2 -1wt%Ni composition. As observed in previous work, the tribological behavior displays a dual-type behavior where the μ changes from a low value (stage 1) to a high value (stage 2). The addition of ~ 1 vol% Al_2O_3 had no significant effect on the TD (Figure 2.6(b)), however the addition of ~ 1 vol% B_4C or BN enhanced the TD slightly. The addition of ~ 6 vol% Al_2O_3 had no effect on the TD. Comparatively, the addition of ~ 5 vol% B_4C or BN had a significant effect on the TD. Figure 2.7(d) summarizes the variation of TD as a function of ceramic particulates content. The TD of Ti_3SiC_2 -1wt% Ni was ~ 10 m. It retained similar values in Ti_3SiC_2 - Al_2O_3 composites. Comparatively, TD increased to ~ 70 m and ~ 250 m in 312Si-5% B_4C and 312Si-5%BN, respectively.

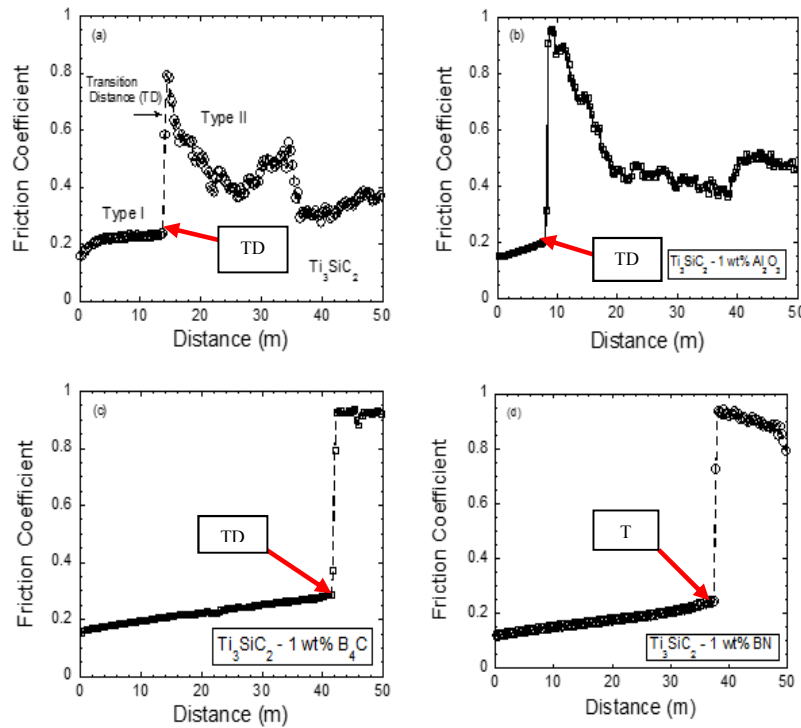


Figure 2.6: Plot of friction coefficient versus distance of, (a) Ti_3SiC_2 -1wt%Ni, (b) 312Si-1% Al_2O_3 , (c) 312Si-1% B_4C and (d) 312Si-1%BN.

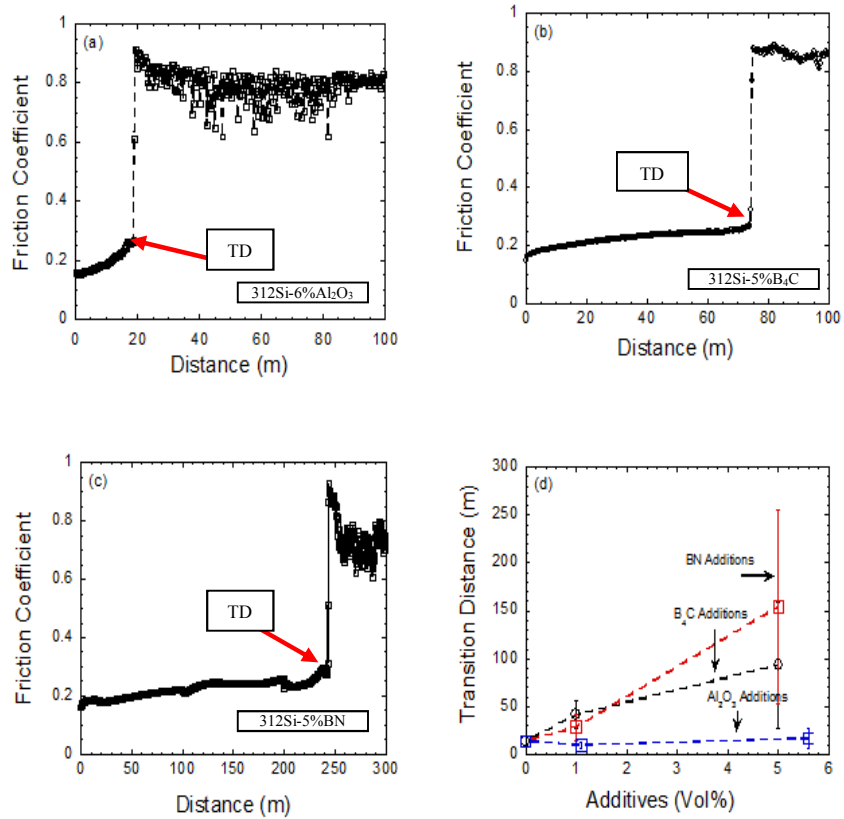


Figure 2.7: Plot of friction coefficient (μ) versus distance of, (a) 312Si-6%Al₂O₃, (b) 312Si-5%B₄C, (c) 312Si-5%BN, and (d) Transition Distance (TD) versus additives (vol%).

This study shows that the microstructure where Ti₃SiC₂ has reacted with the ceramic particulates showed a longer TD. Based on these results, further studies are warranted whether the interpenetrating matrix formed by adding reactive ceramic particulates can further enhance the tribological performance. Figure 2.8 shows a BSE SEM image of stainless steel and 312Si-5%BN wear surface. Both the surfaces are covered with third body debris which is very typical of Type II tribological behavior [10]. More fundamental studies should be focused on minimizing the third body formation.

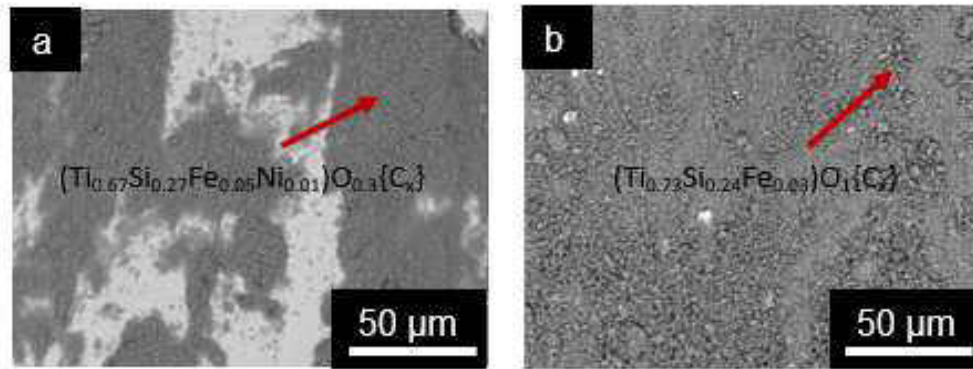


Figure 2.8: BSE SEM micrographs of, (a) stainless steel, and (b) 312Si-5%BN surface after tribological testing.

2.3 - Conclusions

Ti₃SiC₂ matrix composites were fabricated by pressureless sintering by using ~1 wt% Ni as a sintering agent. Ti₃SiC₂ matrix composites were designed by adding ~1 and ~6 vol% Al₂O₃, 1 and 5 vol% BN, and 1 and 5 vol% B₄C ceramics as particulate additives. SEM and XRD studies showed that Al₂O₃ is relatively inert in the Ti₃SiC₂ matrix whereas BN and B₄C reacted significantly with the Ti₃SiC₂ matrix to form TiB₂. Detailed tribological studies showed that Ti₃SiC₂-1wt%Ni samples showed dual type tribological behavior. The addition of Al₂O₃ as a particulate additive had no effect on the TD, but the addition of B₄C and BN particulates were able to enhance the TD. Detailed SEM studies also showed that both the stainless steel and 312Si-5%BN wear surface was covered with third body debris.

CHAPTER III

TiB₂-Ti₃SiC₂ MAXCER COMPOSITES

3.1 - Introduction

This chapter was motivated, in part, by observing the precipitation of TiB₂ in Ti₃SiC₂-B₄C and Ti₃SiC₂-BN composites (please see Chapter II for details). Furthermore, a review of the TiB₂ literature revealed interesting facts about mechanical, tribological, and production-related material attributes [13,22,23]. Very little literature was found incorporating MAX phase materials with TiB₂, and the potential and need for positive TiB₂ material enhancement from a mechanical, tribological and production-related view was apparent. Practical economic limitations, (related to quality, consistency, and cost) curtail more widespread use of TiB₂ beyond current specialized applications, which include armor, cutting tools, crucibles, and wear-resistant coatings [13]. Zheng et.al., and Einarsrud et.al., [23,24] have seen positive mechanical and production-related results with additions of Ni and Ti₃AlC₂ (a MAX phase) to TiB₂.

TiB₂ is a ceramic with high strength and reasonable durability. This characterization is a result of its high melting point (3225 +/-20) °C, hardness, strength to density ratio, and wear resistance [13]. Wide adoption of this material has been limited however, due to its variability of microstructure, low density, and high cost to manufacture [13,23,25] These challenges are primarily due to its high melting point, low self-diffusion coefficient, strong covalent bonding, and low oxidation resistance. Nonetheless, a variety of methods have been proposed and used to compensate for this difficulty in obtaining nearly fully dense polycrystalline TiB₂, such as hot isostatic pressing, microwave sintering, and dynamic compaction [13]. However, with the inherent challenges and expense of the previous methods listed, pressureless sintering of TiB₂

has been attempted, but this method also requires a relatively high sintering temperature (~2000 °C), unfortunately also accelerating grain growth and promoting the formation of a density-inhibiting oxides layer (TiO_2 and B_2O_3) [23]. In order to lower the sintering temperature, some researchers [13,23,25] have added Ni, which is known to reduce sintering temperature requirements, enhance sintering rates, and also suppress grain coarsening. When sintering aids are used in the composition, the theoretical maximum density, ρ_{theo} , can be different from the density of the pure crystal, ρ_{xtal} , because of the differing mass density of the sintering aid and the influence of the sintering aid on the lattice parameters [13,22].

It is with these considerations of past research, that pressureless sintering and sintering aids were chosen to produce a novel TiB_2 -based MAXCER composition. More specifically, Ni is a proven sintering aid, and Ti_3SiC_2 has the potential to form a cementitious network which can result in the improvement of mechanical and tribological performance when combined in various matrix compositions.

3.2 - Experimental Methods

During this study, four different compositions of TiB_2 were designed and manufactured. Specifically, 100 vol% TiB_2 , 90 vol% TiB_2 (TiB_2 -10% Ti_3SiC_2), 70 vol% TiB_2 (TiB_2 -30% Ti_3SiC_2), and 50 vol% TiB_2 (TiB_2 -50% Ti_3SiC_2). Approximately 10 wt% of polyvinyl acetate (PVA) (Part number 363138, Sigma-Aldrich Corp. St. Louis, MO) of the dry weight of the samples were added to all compositions to aid in manufacturing.

The 100 vol% TiB_2 was fabricated without adding any sintering aid. For the 90 vol%, 70 vol%, and 50 vol% TiB_2 compositions, ~1 wt% Ni of the Ti_3SiC_2 content was added as a sintering aid. To manufacture the 100 vol% TiB_2 composition, TiB_2 powder (-325 mesh powder,

Alpha Aesar, Ward Hill MA) was dry ball milled (8000 M mixer Mill, SPEX SamplePrep, Metuchen, NJ) for five minutes, followed by the addition of the PVA, with an additional dry ball milling for 30 seconds. The composition was then poured in a die and cold-pressed ~ 232 MPa (the cycle was repeated twice) in a ~ 12.7 mm die (EQ-Die-12D-B, MTI Corporation, Richmond, CA). To prepare TiB_2 -10% Ti_3SiC_2 , TiB_2 -30% Ti_3SiC_2 , and TiB_2 -50% Ti_3SiC_2 compositions, Ti_3SiC_2 powder (-325 mesh, Kanthal, Hallstahammar, Sweden) and Ni (-325 mesh, Alfa Aesar, Ward Hill MA) were dry ball-milled for five minutes. Thereafter calculated concentrations of the Ti_3SiC_2 -Ni mixture was added to the TiB_2 powder, and dry ball-milled for an additional three minutes. Subsequently, the PVA was added to the powders, with a final 30 seconds of further dry ball-milling. Similar to above mentioned procedure, the mixture was then poured in a die, and cold-pressed at ~ 232 MPa (the cycle was repeated twice) in a ~ 12.7 mm die (EQ-Die-12D-B, MTI Corporation, Richmond, CA). All compositions were sintered at 1550 °C for 120 minutes at a ramp rate of 10 °C /min in a tube furnace with Ar flowing through it (to prevent oxidation of the sample.)

The rule of mixtures was used to calculate the theoretical density of all the composite samples, by using the theoretical density of TiB_2 and Ti_3SiC_2 (MAX phase) particulates. The experimental density was determined from the mass and dimensions of each sample. The relative density was then calculated by normalizing the experimental density with the theoretical density. As in Chapter II, the theoretical density was calculated from the density of the precursor powders as PIs do not have the experimental means to calculate the interfacial reactions. Thus, the porosity calculations should be used for qualitative comparison. All the composites were polished ($R_a < 1$ μm) and then tested by a Vicker's micro-hardness indenter (Mitutoyo HM-112,

Mitutoyo Corporation, Aurora, IL) by loading the samples at 9.8 N for 12 seconds, and an average of five readings for each composite system is reported in the text.

The phase analysis was performed by XRD (SmartLab, Rigaku, Japan) at a scan rate of 0.05 °/min from 20° to 70°. The tribological behavior of the samples were tested by using a ball-on-disc tribometer (CSM Instruments SA, Peseux, Switzerland) at 5 N, 25 m, ~25 cm/s linear speed, and ~4 mm track radius against stainless steel balls.

The microstructure of the samples was studied by using a JEOL JSM-6490LV Scanning Electron Microscope (SEM JEOL USA, Inc., Peabody, Massachusetts) in Secondary Electron (SE) and Backscattered Electrons (BSE) mode. The chemical information was obtained by X-ray analysis via a Thermo Nanotrace Energy Dispersive X-ray detector with NSS-300e acquisition engine.

3.3 - Results and Discussion

In Figure 3.1, SEM images of the fracture surfaces of 100 vol% TiB₂, (a and b) TiB₂-10%Ti₃SiC₂ (c and d), TiB₂-30%Ti₃SiC₂ (e and f), and TiB₂-50%Ti₃SiC₂ (g and h) are shown. The Ti₃SiC₂ particulates are well dispersed in the TiB₂ matrix. Pores between the grains can be observed in Figure 3.1(a), principally due to the low density of monolithic TiB₂, as well as in Figure 3.1(b), showing residue from the diamond polish due to the porous nature of the TiB₂ grains. When 30 vol% and 50 vol% Ti₃SiC₂ were added to the TiB₂, the densification of the TiB₂ matrix were remarkably improved, as shown in Figure 3.1(e) and 3.1(g).

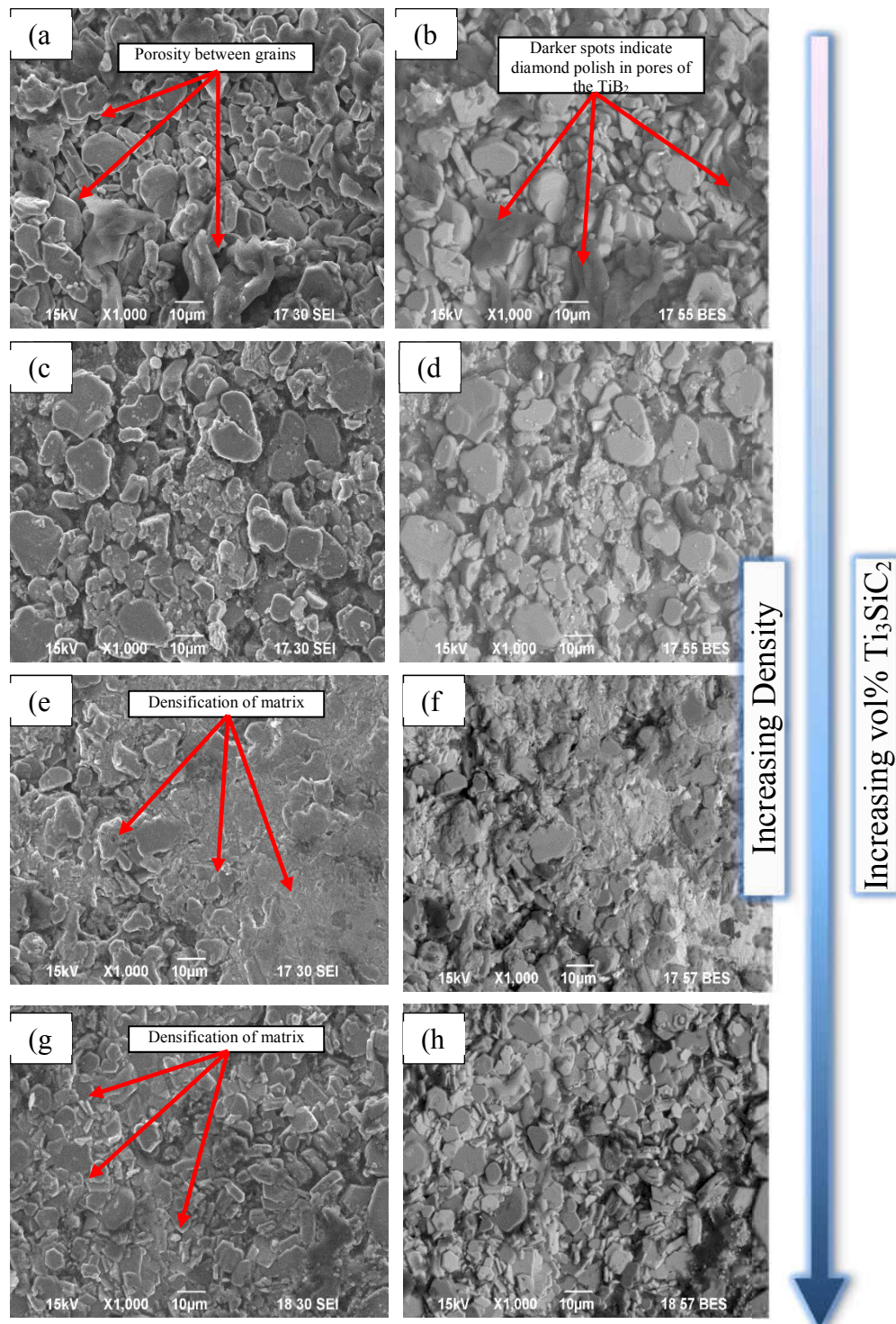


Figure 3.1: SE SEM images of (a) TiB_2 , (b) BSE of the same image (dark phase is the porosity in which diamond polish has entered the pores), (c) TiB_2 -10% Ti_3SiC_2 , (d) BSE of the same image, (e) TiB_2 -30% Ti_3SiC_2 , (f) BSE of the same image, (g) TiB_2 -50% Ti_3SiC_2 , and (h) BSE of the same image.

Figure 3.2 summarizes the XRD profile of all the compositions. The profiles show good stability of the composite with Figure 3.2(a)-(d) being the TiB_2 , TiB_2 -10% Ti_3SiC_2 , TiB_2 -30% Ti_3SiC_2 , TiB_2 -50% Ti_3SiC_2 , respectively.

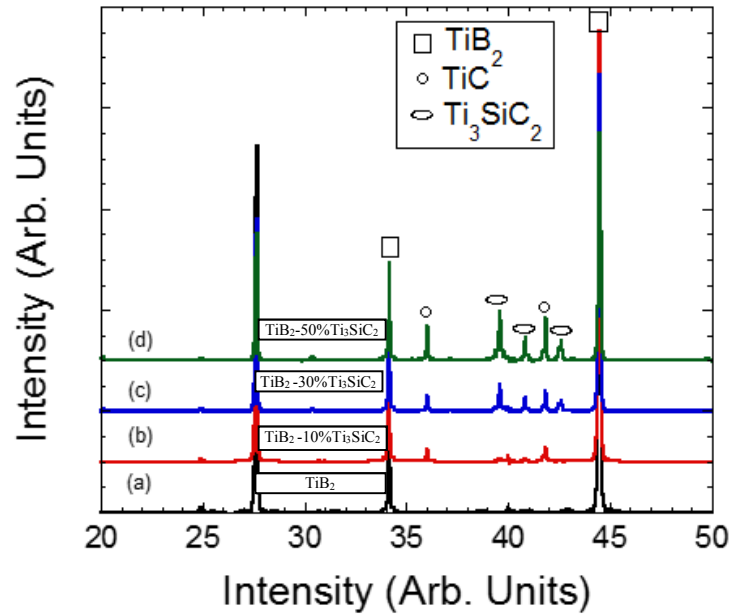


Figure 3.2: XRD analysis of (a) TiB_2 , (b) TiB_2 -10% Ti_3SiC_2 , (c) TiB_2 -30% Ti_3SiC_2 , and (d) TiB_2 -50% Ti_3SiC_2 .

Figure 3.3 (left), shows the plot of relative density versus the additions of MAX particulates. 100% TiB_2 resulted in rather poor $\sim 63\%$ relative densification. With the increasing additions of Ti_3SiC_2 , the relative density increased to $\sim 71\%$ for TiB_2 -10% Ti_3SiC_2 , $\sim 78\%$ for TiB_2 -30% Ti_3SiC_2 , and $\sim 82\%$ for TiB_2 -50% Ti_3SiC_2 . Overall, relative density increased with additions of Ti_3SiC_2 , as shown in Figure 3.3 (left).

The hardness of 100% TiB₂ was ~7.3 GPa, TiB₂-10%Ti₃SiC₂ was ~6.5 GPa, and TiB₂-30%Ti₃SiC₂ was ~6.1 GPa. The TiB₂-50%Ti₃SiC₂ showed an increase in hardness at ~7.7 GPa. The hardness trends can be seen in Figure 3.3 (right).

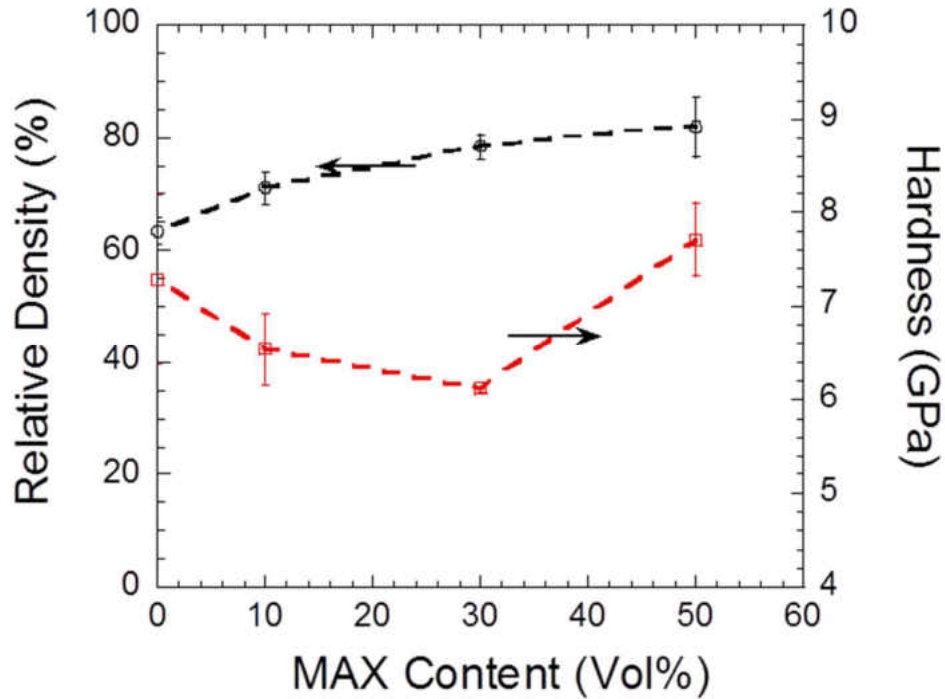


Figure 3.3: Relative Density and Hardness versus MAX Content (vol%).

Figure 3.4 shows a reasonably low μ_{mean} for all compositions. Specifically, μ_{mean} was ~0.3 in TiB₂ and TiB₂-10%Ti₃SiC₂, increased to ~0.45 in TiB₂-30%Ti₃SiC₂, and finally decreased to ~0.15 in TiB₂-50%Ti₃SiC₂. Figure 3.5 shows the μ versus distance profiles of Ti₂B₂-Ti₃SiC₂ composition. The (0, 10, and 30) vol% Ti₃SiC₂-Ni mixtures all display similar tribological responses profiles. Figure 3.6 shows quantitatively that 100% Ti₂B₂ showed the greatest wear rate ~0.067 mm³/Nm, and then decreased to ~0.0007 mm³/Nm in TiB₂-10%Ti₃SiC₂. Thereafter it increased sharply to 0.023 mm³/Nm in TiB₂-30%Ti₃SiC₂, and finally it decreased in TiB₂-

50%Ti₃SiC₂, which showed a very low wear rate at $\sim 9.8 \times 10^{-5} \text{ mm}^3/\text{Nm}$. At this juncture, it is not clear what is the exact mechanism for this erratic behavior. Further studies are needed to understand the exact mechanism.

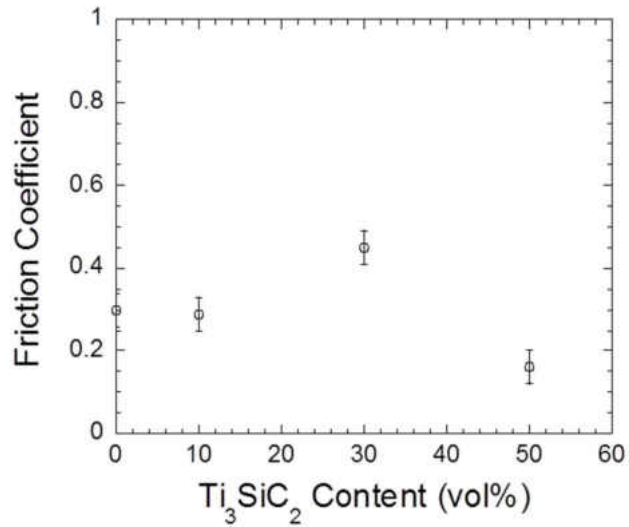


Figure 3.4: Friction coefficient versus Ti₃SiC₂ vol%.

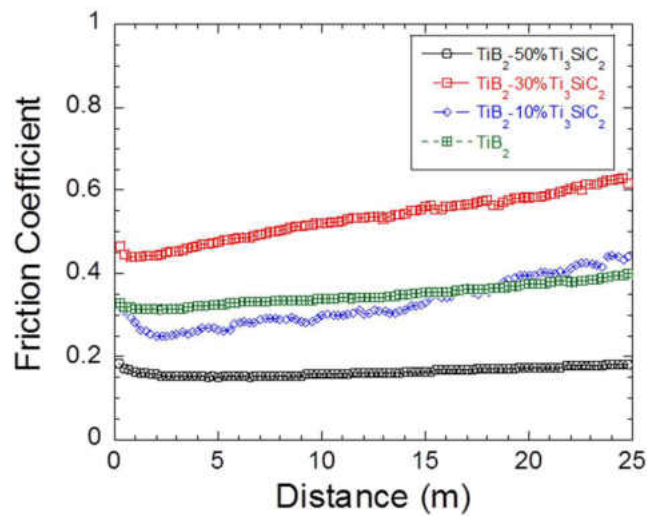


Figure 3.5: Friction coefficient versus sliding distance (25 m).

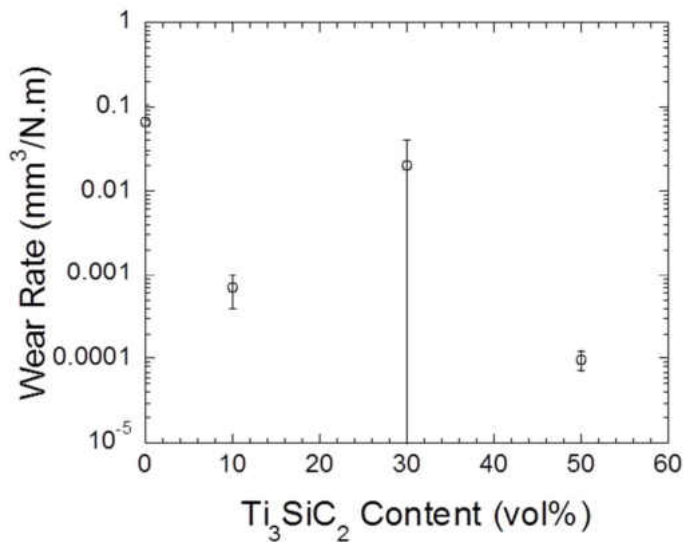


Figure 3.6: Wear rate versus Ti₃SiC₂ content (vol%).

For qualitative purposes, Figure 3.7 shows an SE and BSE SEM image of TiB₂-10%Ti₃SiC₂ wear surface. As expected, because of the high hardness of the TiB₂-10%Ti₃SiC₂ relative to the stainless steel, Fe is the main constituent of the tribofilms as shown in Figure 3.7(b). Clearly, based on above mentioned results, the TiB₂-50%Ti₃SiC₂ composite showed the most promising tribological behavior. Figure 3.8 shows the long term testing of this composition for 1000 m. Interestingly, in all cases, the μ transitioned to a higher value of >0.6 which indicates that the low μ is stable for low cycling times. Interestingly, the WR after cycling for 1000 m was 0.0003 ± 0.0004 mm³/Nm which is only marginally higher than cycling for 25 m $\sim 9.8 \times 10^{-5}$ mm³/Nm. Additional fundamental studies should be focused on minimizing the third body formation. Finally, even though this study chose not to use any sintering aid in the 100 vol% TiB₂ samples to establish a baseline porosity using pressureless sintering, further studies should include a sintering aid such as Ni to facilitate experimentally practical results.

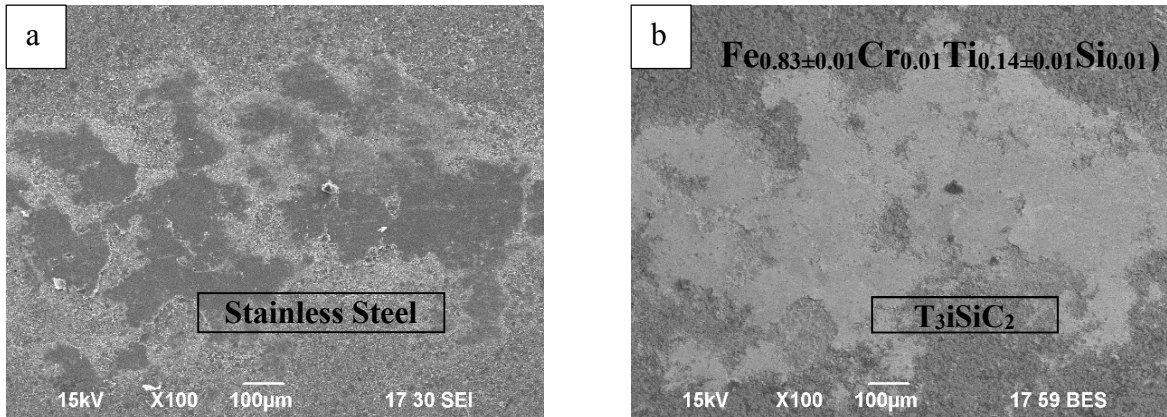


Figure 3.7: SEM micrograph of tribofilm formed on TiB_2 -10% Ti_3SiC_2 surface.

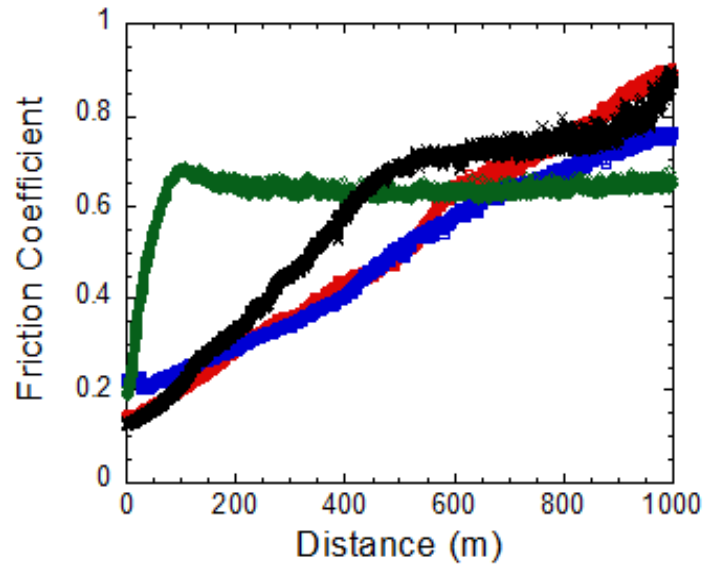


Figure 3.8: Experimental runs of friction versus sliding distance of TiB_2 -50% Ti_3SiC_2 (1000 m).

3.4 – Scope for Future Studies

During all the studies, Ti_3SiC_2 was added to a variety of ceramics creating different ceramic-matrix composites. Due to Ti_3SiC_2 being the only MAX phase material used, it is recommended for further investigation to focus on adding different A group and M group elements, creating other novel MAXCERs. Finally, observing the high temperature capabilities of ceramics in general and looking at the excellent elevated temperature tribological results of certain MAX phase materials such as Ti_3SiC_2 , High Temperature (HT) studies might also reveal promising results.

APPENDIX

References

- [1] Z. Li, A. Zhou, L. Liang, W. Libo, H. Meihua, L. Shangsheng, S. Gupta, "Synthesis and characterization of novel Ti₃SiC₂-cBN composites," *Diamond & Related Materials*, no. 43, pp. 29-33, 2014.
- [2] M.W. Barsoum, "Introduction" in *Fundamentals of Ceramics*, New York, NY, Taylor and Francis Group, 2003, pp. 6-7.
- [3] M. W. Barsoum, T. El-Raghy. "Synthesis and Characterization of a Remarkable Ceramic: Ti₃SiC₂," *Journal of the American Ceramic Society*, vol. 79, no. 7, pp. 1953-1956, 1996.
- [4] M.W. Barsoum, M. Radovic, "Elastic and Mechanical Properties of the MAX Phases", *Annu. Rev. Mater. Res.*, vol. 41, pp. 195-227, 2011.
- [5] M. W. Barsoum, "The MN+1AXN phases: A new class of solids: Thermodynamically stable nanolaminates," *Progress in Solid State Chemistry*, vol. 28, no. 1-4, pp. 201-281, 2000.
- [6] S. Myhra, J.W.B. Summers, E.H. Kisi, "Ti₃SiC₂ - a layered ceramic exhibiting ultra-low friction," *Material Letters*, pp. 6-11, 1999.
- [7] T. El-Raghy, P. Blau, M.W. Barsoum, "Effect of grain size on friction and wear behavior of Ti₃SiC₂," *Wear*, vol. 238, no. 2, pp. 152-130, 2000.
- [8] P. Blau, "Interpretations of the friction and wear break-in behavior of metals in sliding contact," *Wear*, p. 29, 1981.
- [9] A.Souchet, J. Fontaine, M. Meline, T. Le-Mogne, M.W. Barsoum, "Tribological duality of Ti₃SiC₂" *Tribology Letters*, pp. 341-352, 2000.
- [10] S. Gupta, M.W. Barsoum "On the tribology of the MAX phases and their composites during

- dry sliding: A review," *Wear*, vol. 271, no. 9-10, pp. 1878-1894, 2011.
- [11] M. W. Barsoum, "Introduction" in *Fundamentals of Ceramics*, New York, NY, Taylor and Francis Group, 2003, pp. 6-7.
- [12] W. Hillig, "Strength and Toughness of Ceramic Matrix Composites," *Annual Review of Material Science*, pp. 341-383, 1987.
- [13] R. Munro, "Material Properties of Titanium Diboride," *Journal of Research of the National Institute of Standards and Technology*, vol. 105, no. 5, pp. 709-720, 2000.
- [14] Z. Liya, F. Li, Y. Zhou, "Preparation, Microstructure, and Mechanical Properties of TiB₂ Using Ti₃AlC₂ as a Sintering Aid," *Journal of the American Ceramic Society*, vol. 95, no. 6, pp. 2028-2034, 2012.
- [15] Z. Li, A. Zhou, L. Li, W. Libo, H. Meihua, L. Shangsheng, S. Gupta, "Synthesis and characterization of novel Ti₃SiC₂-cBN composites," *Diamond & Related Materials*, no. 43, pp. 29-33, 2014.
- [16] J. Jianfeng, T. Rong, G. Takashi, "Densification, microstructure and mechanical properties of SiO₂-cBN composites by spark plasma sintering," *Ceramics International*, pp. 351-356, 2012.
- [17] C.A. CARACOSTAS, W.A. Chiou, M.E. Fine, H.S. Cheng, "Tribological Properties of Aluminum Alloy Matrix TiB₂ Composite Prepared by In Situ Processing," *METALLURGICAL AND MATERIALS TRANSACTIONS*, p. 491, 1997.
- [18] T.P. Herbell, J.W. Weeton, M. Quatinetz, "Structure and Properties of Tungsten-Base Powder Metallurgy Composites," NASA, Cleveland, 1966.
- [19] C.A. Caracostas, W.A. Chiou, M.E. Fine, H.S. Cheng, "Tribological Properties of Aluminum Alloy Matrix TiB₂ Composite Prepared by In Situ Processing," *METALLURGICAL AND MATERIALS TRANSACTIONS*, p. 491, 1997.

- [20] A. Moghadam, "Functional Metal Matrix Composites: Self-lubricating, Self-healing, and Nanocomposites-," *Journal of Materials*, pp. 872-881, 2014.
- [21] T. Rainer, A. Momozawaa, D. Musicb, J. M. Scheiderb, "Boride-based nano-laminates with MAX-phase-like behaviour," *Journal of Solid State Chemistry*, pp. 2850-2857, 2006.
- [22] V.J.Tennery, C.B. Finch, G.W. Clark, "Structure-Property Correlations for TiB₂-Based Ceramics Densified Using Active Liquid Metals, in Science of Hard Materials," NY, New York, Plenum, 1981, pp. 891-909.
- [23] B.B. Panigraha, N. S. Reddy, A. Balakrishnan, M.-C. Chu, S.-J. Cho, J.J. Gracio, "Nickel assisted sintering of Ti₃SiC₂ powder under pressureless conditions," *Journal of Alloys and Compounds*, no. 505, pp. 337-342, 2010.
- [24] P. Eklund, M. Beckers, U. Jansson, H. Hogberg, L. Hultman, " The M_{n+1}AX_n phases: Materials science and thin-film processing" *Journal of Thin Solid Films*, no. 518, pp 1851-1878, 2010.
- [25] M.W. Barsoum, *Fundamentals of Ceramics*, New York, NY: Taylor & Francis Group, 2003.
- [26] M.W. Barsoum, "MAX Phases: Properties of Machinable Ternary Carbides and Nitrides", John Wiley & Sons , 2013.
- [27] M. W. Barsoum, "The MN+1AXN phases: A new class of solids: Thermodynamically stable nanolaminates," *Progress in Solid State Chemistry*, vol. 28, no. 1-4, pp. 201-281, 2000.
- [28] M. W. Barsoum, T. El-Raghy, "The MAX Phases: Unique New Carbide and Nitride Materials," *American Scientist*, vol. 89, no. 4, pp. 334-343, 2001.
- [29] M.W. Barsoum, T. Zhen, M. Radovic, A. Muruqaiah, "Fully reversible, dislocation-based compressive deformation of Ti₃SiC₂ to 1 GPa," *Nature Materials*, vol. 2, no. 1, pp. 107-111, 2003.

- [30] M.W. Barsoum, T. El-Raghy, "Synthesis and Characterization of a Remarkable Ceramic: Ti_3SiC_2 ," *Journal of the American Ceramic Society*, vol. 79, no. 7, pp. 1953-1956, 1996.
- [31] J.S. Myhrea, J.W.B. Summersb, E.H. Kistic, " Ti_3SiC_2 —A layered ceramic exhibiting ultra-low friction," *Materials Letters*, vol. 39, no. 1, pp. 6-11, 1999.
- [32] P. Blau, "Interpretations of the friction and wear break-in behavior of metals in sliding contact," *Wear*, pp. 29, 1981.
- [33] A. D. Moghadam, "Functional Metal Matrix Composites: Self-lubricating, Self-healing, and Nanocomposites-," *Journal of Materials*, pp. 872-881, 2014.
- [34] L. Zheng, L. Fangzhi, Z. Yanchun, "Preparation, Microstructure, and Mechanical Properties of TiB_2 Using Ti_3AlC_2 as a Sintering Aid," *Journal of the American Ceramic Society*, vol. 95, no. 6, pp. 2028-2034, 2012.
- [35] D.L. Zhangw, Z.H. Cai, A.J. Huang, R. Yang, "Synthesis, Microstructure, and Mechanical Properties of a Novel $Ti_2AlC/TiC/Al_2O_3$ In Situ Composite," *Journal of American Ceramic Society*, pp. 3325-3330, 2006.
- [36] T. El-Raghya, P. Blaub, M.W. Barsoum "Effect of grain size on friction and wear behavior of Ti_3SiC_2 ," *Wear*, vol. 238, no. 2, pp. 152-130, 2000.

